



Site-Specific Relationships between Bedrock Depth and HVSR Fundamental Resonance Frequency Using KiK-NET Data from Japan

MOSTAFA THABET¹

Abstract—It is commonly accepted that the horizontal-to-vertical spectral ratio (HVSR) technique enables the detection of the fundamental resonance frequency (f_{HVSR}) of a given site. The utility of this f_{HVSR} is analyzed using the nonlinear regression relationships between f_{HVSR} and bedrock depth (h). The derived relationships are mostly site-specific, so that the present paper consists of two main parts. The first is a literature review for the available empirical relationships between f_{HVSR} and h . The aim of this part is to highlight the practical limitations of these established relationships and to make fair comparisons. The second is to generate new relationships, taking advantage of the very wide range of available lithological, geophysical, and geotechnical borehole drilling data of the 697 KiK-NET seismic stations in Japan. For this purpose, HVSR are calculated using 10,000 weak earthquakes or linear events recorded at KiK-NET stations to determine the f_{HVSR} and correlate it with the corresponding h . The overlying layers/bedrock interface falling within sedimentary, igneous, or metamorphic layers significantly affect the derived frequency–depth relationships. In addition, these relationships are strongly reproduced by the V_p/V_s ratio of the bedrock in the range of 1.6–2.2. Interestingly, it is found that f_{HVSR} less than 1 Hz corresponding to h more than 100 m leads the trend of the overall frequency–depth relationship.

Key words: H/V spectral ratio, geophysical exploration, seismic site classification, bedrock depth, KiK-NET (Japan).

1. Introduction

The horizontal-to-vertical spectral ratio (HVSR) technique (Nogoshi and Igarashi 1970, 1971; Nakamura 1989, 2000) has been studied extensively using both simulations and comparisons with earthquake recordings to quantify the site effects produced by the sedimentary covering in specific frequency bands (Field and Jacob 1993; Lachet and Bard 1994; Lermo

and Chavez-Garcia 1994; Bindi et al. 2000; Fäh et al. 2001). These studies show that when a large impedance contrast exists between the sediments and the bedrock, the peak in the HVSR can be used to estimate the fundamental resonance frequency (f_{HVSR}) of a site. Lermo and Chavez-Garcia (1993) proved that the HVSR technique can also be applied to the strongest part of the earthquake recordings (S waves). Since then, many studies (Lachet and Bard 1994; Castro et al. 1997; Mucciarelli 1998; Parolai et al. 2004) have been accomplished to determine the applicability and the limitations of the HVSR technique both for earthquakes and seismic noise.

The utility of the f_{HVSR} can be analyzed using nonlinear regression relationships between this f_{HVSR} of a given site, its bedrock depth (h), and the average shear wave velocity ($\overline{V_s}$). As a result, this application can quickly obtain a general idea of the subsurface structure, particularly in regions of unknown bedrock topography.

The seismic response at the surface of soil deposits is dependent mainly on the frequency content and amplitude of ground motion at the bedrock. Seismic site classification methods consider average values of shear wave velocities and standard penetration test values (N value) of the top 30 m soil layer according to the National Earthquake Hazards Reduction Program (NEHRP) (FEMA 222A 1994; FEMA 450 2004) and International Building Code (IBC) (2009) classification systems. Site classification has also been carried out by considering the depth of bedrock. Anbazhagan and Sitharam (2009) considered shear wave velocities of 700 ± 60 m/s, where there are N values of 100 for no penetration, as the signature of bedrock that represents a stiffer soil

¹ Seismology Lecturer, Geology Department, Faculty of Science, Assiut University, Assiut 71516, Egypt. E-mail: mostafa.thabet@aun.edu.eg; mostafa.thabet@science.au.edu.eg

column as adopted in the design codes of the different site classification approaches.

The first part of this paper reviews available relationships between the f_{HVSr} and h . The existing relationships were established by Ibs-von Seth and Wohlenberg (1999), Delgado et al. (2000a, b), Parolai et al. (2002), Hinzen et al. (2004), Birgören et al. (2009), Özalaybey et al. (2011), Harutoonian et al. (2013), Fairchild et al. (2013), Del Monaco et al. (2013), and Tün et al. (2016). A detailed summary of these relationships is presented with comparisons. In the second part of this paper, new relationships are developed, considering a large variety of valuable seismological, geotechnical, lithological, stratigraphical, and geological conditions provided from the KIBAN Kyoshin network (KiK-NET) seismic stations in Japan. It is important to note that all these previous studies depended on ambient vibrations or microtremor measurements, whereas the present study will depend on weak earthquakes or linear events to avoid the complexities of nonlinear responses. Yamanaka et al. (1994) investigated inference of subsurface structure using measurements of long-period microtremors in the northwestern part of the Kanto Plain in Japan, where sediment thickness varied from 0 to 1 km. They found that the ellipticities of Rayleigh waves in earthquake ground motions were consistent with those of the microtremors in peak periods and amplitudes. Bard and the SESAME team (2004) compared HVSr curves calculated using ambient vibrations and standard-spectral-ratio (SSR) curves calculated using earthquakes. Their results show overall good agreement between the HVSr and SSR curves in the fundamental resonance frequencies derived from each method. Based on these studies, KiK-NET data for weak earthquakes are used in this study.

Finally, comparisons are discussed between previously established frequency–depth relationships and those newly developed from the present study.

2. Existing Relationships between Bedrock Depth and Resonance Frequency

One of the most common approaches used to estimate bedrock depth is based on nonlinear

regression relationships of bedrock depth versus fundamental resonance frequency. These regression relationships are site-specific.

The first studies by Yamanaka et al. (1994) and Field (1996) demonstrated that the bedrock depth (i.e. the thickness of the overlying soft sediment layers) can be directly evaluated from the fundamental resonance frequency, measured by the HVSr of microtremors. Ibs-von Seth and Wohlenberg (1999), Delgado et al. (2000a, b), and Parolai et al. (2002) adopted the frequency–depth approach to evaluate bedrock depth (h) using the fundamental resonance frequency (f_{HVSr}), through the following relationship

$$h = a f_{\text{HVSr}}^{-b} \quad (1)$$

where a and b are curve-fitting parameters.

Based on previously established studies at different locations around the world, the curve-fitting parameters a and b are summarized in Table 1. Ibs-von Seth and Wohlenberg (1999) investigated the application of Nakamura's technique and transfer function technique using microtremor measurements to determine sediment thicknesses in the western Lower Rhine Embayment (Germany). The frequencies and sediment thicknesses determined in this previous study were limited to ranges of 5–0.1 Hz and 15–1600 m, respectively. The impedance contrasts for the soft sediments overlying hard bedrock were approximately the same at all sites in the Lower Rhine Embayment study area.

One year later, Delgado et al. (2000a, b) conducted their studies at two different survey locations in Segura River Valley (southeastern Spain). They investigated 180 and 33 microtremor sites in the first and the second studies, respectively. Their studies can be considered shallow studies because the maximum investigated bedrock depth was 44.7 m. The determined fundamental resonance frequencies ranged from 1.1 Hz to 8.3 Hz.

Parolai et al. (2002) carried out noise measurements at 32 sites in the Cologne area (Germany), focused on obtaining a subsoil classification for seismic hazard assessment. They established relationships of V_s versus bedrock depth and bedrock depth versus fundamental resonance frequency within frequency and bedrock depth ranges of 0.25–20 Hz and 500–2 m, respectively.

Table 1
Existing correlation coefficients or curve-fitting parameters of frequency-depth relationships

Location	Study	a	b	R_s	No. of data sites	f_{HVSR} range (Hz)	h range (m)	Remarks
Lower Rhine Embayment, Germany	Ibs-von Seth and Wohlenberg (1999)	96	1.388	0.98	102	0.10–5.0	15–1600	(1) HVSR
		146	1.375	0.75				(2) Transfer function
Segura River Valley, Southeastern Spain	Delgado et al. (2000a)	55.11	1.256	0.97	180	1.16–8.3	4.1–43.5	
Cologne area, Germany	Delgado et al. (2000b)	55.64	1.268	0.98	33	1.10–8.3	4.1–44.7	
Lower Rhine Embayment, Germany	Parolai et al. (2002)	108	1.551		337	0.25–20	2–500	
	Hinzen et al. (2004)	137	1.190	0.96	152	0.20–2.5	10–1200	
Southern coast of Istanbul, Turkey	Birgören et al. (2009)	150.99	1.153	0.995	15	0.4–1.54	20–449	
Izmit Bay area, Turkey	Özalaybey et al. (2011)	141	1.270	0.91	239	0.25–3.8	20–1100	
Western Sydney, Australia	Harutoonian et al. (2013)	73	1.170	0.94	15	4.2–27	1.2–13.3	
Cape Cod, Massachusetts, USA	Fairchild et al. (2013)	90.53	1.000	1.00	164	0.73–2.43	118–460	
L'Aquila, central Italy	Del Monaco et al. (2013)	53.461	1.01	0.41	25	4–10	3–< 20	
Eskisehir Quaternary Basin, Turkey	Tün et al. (2016)	136	1.357	0.985	30	0.30–15	0–500	
Japan	This study	117.13	1.197	0.94	224	0.095–22.5	2–1500	Sedimentary bedrock
		105.14	0.899	0.62	64	0.198–17.13	4–625	Igneous bedrock
		132.67	1.084	0.90	36	0.304–12.55	6–550	Metamorphic bedrock
		116.62	1.169	0.98	55	0.095–22.5	3.5–1500	Sedimentary bedrock with $V_p/V_s = 1.6\text{--}2.2$

Hinzen et al. (2004) determined the sediment thickness across an active normal fault (i.e. Erft-Sprung normal fault system) in the Lower Rhine Embayment (Germany). They measured the ambient seismic vibrations at 152 sites along two profiles. The resulting fundamental resonance frequencies were limited to between 0.2 Hz and 2.5 Hz to determine a comprehensive empirical relation for corresponding thicknesses between 1200 m and 10 m.

Birgören et al. (2009), Özalaybey et al. (2011), and Tün et al. (2016) recently investigated the relationships of bedrock depth versus fundamental resonance frequency at three different localities in Turkey. The maximum bedrock depths on the southern coast of Istanbul and in the Eskisehir Quaternary basin are 449 m and 500 m, respectively, while the Izmit bay area is 1100 m. Their obtained parameters (i.e. a and b) were very close to each other.

Harutoonian et al. (2013) conducted their study in a dynamically compacted fill area in western Sydney. Their HVSR microtremor measurements yielded

resonance frequencies in the range of 4.2–27 Hz, corresponding to bedrock depths of 13.3–1.2 m. They used the secondary resonance frequencies at higher frequency bands that may reflect strong impedance contrast within surface layers. They verified their results by independent mechanical tests.

In the same year, Fairchild et al. (2013) carried out a study to map the bedrock topography in western Cape Cod, Massachusetts (USA). They conducted HVSR microtremor measurements at 164 sites, verifying bedrock depths using borings drilled to bedrock and seismic refraction surveys.

Additionally, Del Monaco et al. (2013) established a frequency–depth relationship to determine the thicknesses of the surface soil weathered breccia. They obtained the frequency from a detailed seismic noise survey carried out in historical downtown L'Aquila after the earthquake of 6 April 2009 ($M_w = 6.3$). Their measurements at 25 borehole logs yielded resonance frequencies in the range of 4–10 Hz, corresponding to bedrock depths of 20–3 m.

Review shows that these previous valuable studies were carried out at a local scale. Studies by Ibs-von Seth and Wohlenberg (1999), Parolai et al. (2002), and Hinzen et al. (2004) all focused on the Lower Rhine Embayment in Germany, whereas studies by Delgado et al. (2000a, b) focused in the south and on the southeastern coast of Spain. Although studies conducted by Birgören et al. (2009), Özalaybey et al. (2011), and Tün et al. (2016) were carried out at three different localities in Turkey, the resulting curve-fitting parameters a and b were very similar. Some of these studies had limitations in data sites, fundamental resonance frequencies, or bedrock depths. For example, Birgören et al. (2009) determined 1.54 Hz as the maximum fundamental resonance frequency, and Delgado et al. (2000a) established their relationship using maximum bedrock depth of 43.5 m.

The similarities in the b values may be an indication that this parameter is of low variability, while a values would actually be a characteristic parameter for each region (i.e. site-specific parameter). However, this review shows that much caution must be taken before applying these previously established relationships at any region, since it is possible that these relationships are restricted not only to their studied locations, but also to their studied bedrock depths and resonance frequencies. This means that in the case that these relationships are applied within their original locations exceeding their maximum depths or frequencies, layers of velocities and depths may occur that deviate much more or much less from their derived frequency–depth relationships.

3. Data Set

To conduct the present study, the KIBAN Kyoshin network (KiK-NET) was chosen, which has both borehole and surface seismographs. KiK-NET consists of 697 observation stations, and Fig. 1 shows the distribution of KiK-NET seismic stations in Japan. KiK-NET is an open data network (<http://www.kik.bosai.go.jp>). Because of the lack of available geotechnical and seismological data at 13 KiK-NET stations, 684 of the 697 stations are used in the present analyses.

In the present study, three-component records of more than 10,000 earthquakes at the surface of the 684 KiK-NET stations are used for the analyses. It is worth mentioning that the earthquakes used in this study do not include strong motions or nonlinear events, thus avoiding the added complexity of later modification due to nonlinear responses. The accelerations recorded at the surface of the KiK-NET stations used in the analyses range between 68.03 cm/s^2 and 0.02 cm/s^2 .

There are two main reasons for choosing the KiK-NET data. First, P -wave and S -wave velocity profiles, with their geological information, are available for depths between 100 m and 3500 m. Six hundred thirteen of the KiK-NET stations have borehole depths less than 250 m, while 42 stations have borehole depths between 250 m and 500 m. There are also 42 deeper boreholes (more than 500 m in depth) that are constructed on thick sediment within large plains, such as Kanto plain or Osaka basin. As a result, it will be possible to define the bedrock. Second, these 684 KiK-NET stations cover a large variety of geological and lithological conditions. Some stations have bedrock depths that can be found within sedimentary, igneous, or metamorphic layers.

4. HVSr Processing

This section describes the detailed procedure for the HVSr calculation and the bedrock depth characterization. This procedure consists of eight main steps. These steps are summarized as shown in Fig. 2, and are discussed in detail as follows:

1. Estimating the bedrock depths at each KiK-NET station

In the present study, the seismic impedance contrasts between each adjacent two layers are calculated at each KiK-NET station using $(IC_P = (\sigma V_P)_{\text{underlying layers}} / (\sigma V_P)_{\text{overlying layers}})$ for P -wave velocities and $(IC_S = (\sigma V_S)_{\text{underlying layers}} / (\sigma V_S)_{\text{overlying layers}})$ for S -wave velocities. The first and second highest impedance contrasts indicate the potential presence of the bedrock interfaces. The reason for using the second highest impedance contrast is that many KiK-NET stations have very

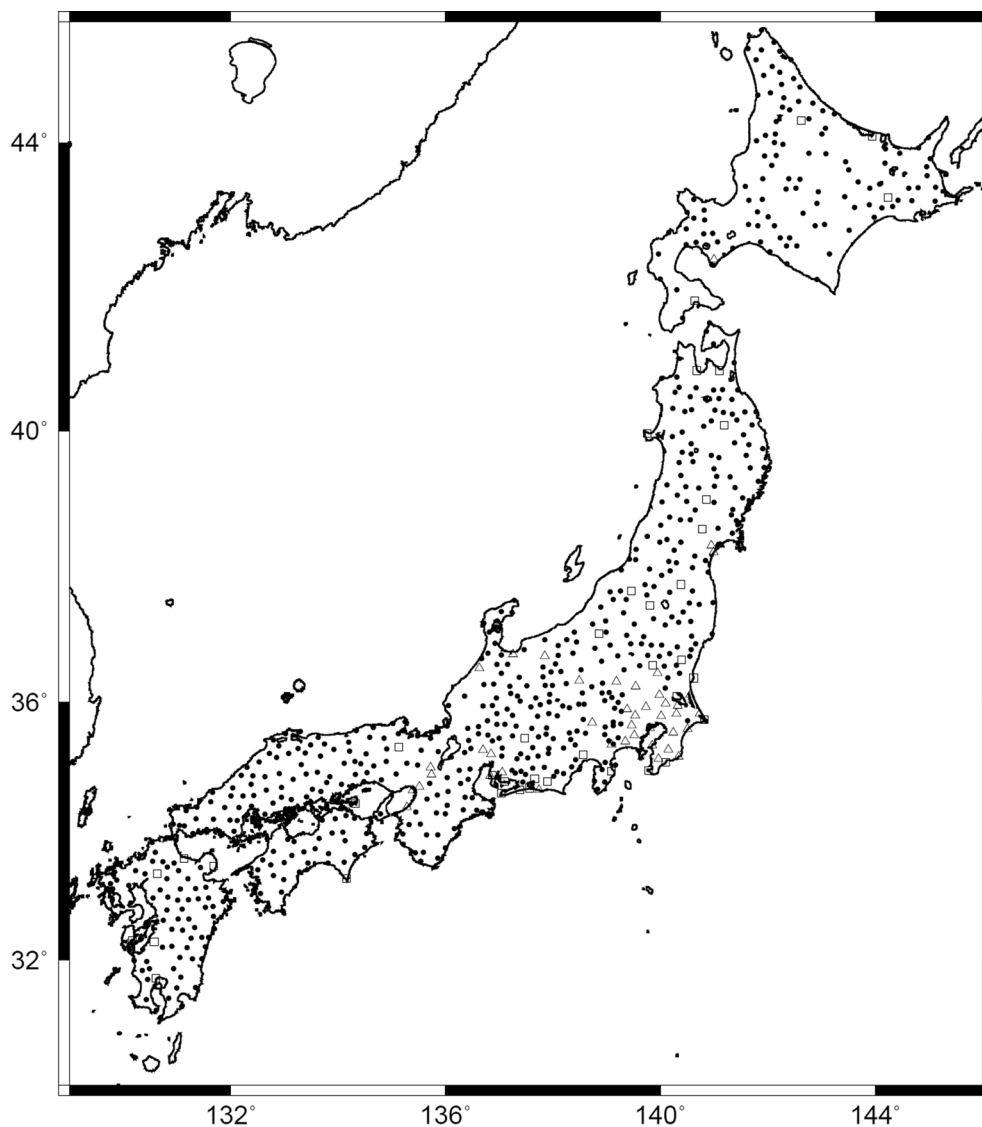


Figure 1

Location of the 697 KiK-NET seismic stations in Japan. Solid circles, open squares, and open triangles are stations with borehole depths < 250 m, 250–500 m, and > 500 m, respectively

surficial layers (i.e. top few meters). These surficial layers can yield the first highest impedance contrast, whereas the second highest impedance contrast indicates the presence of the reliable deep bedrock interface which is responsible for the fundamental resonance frequency. It is important to note that this step is a preliminary step for estimating the bedrock depth. In the seventh step of this HVSR procedure, the appropriate bedrock depths are assigned to their

corresponding fundamental resonance frequencies, while the unreasonable bedrock depths are excluded from any further analyses.

Yoshimura et al. (2003) and Maeda (2004) carried out microtremor array observations for Rayleigh wave phase-velocity dispersion curves and found that shear wave velocities within a near-surface, thin, and soft layer are likely to be lower than those derived by *PS* logging data. This means that the shear wave

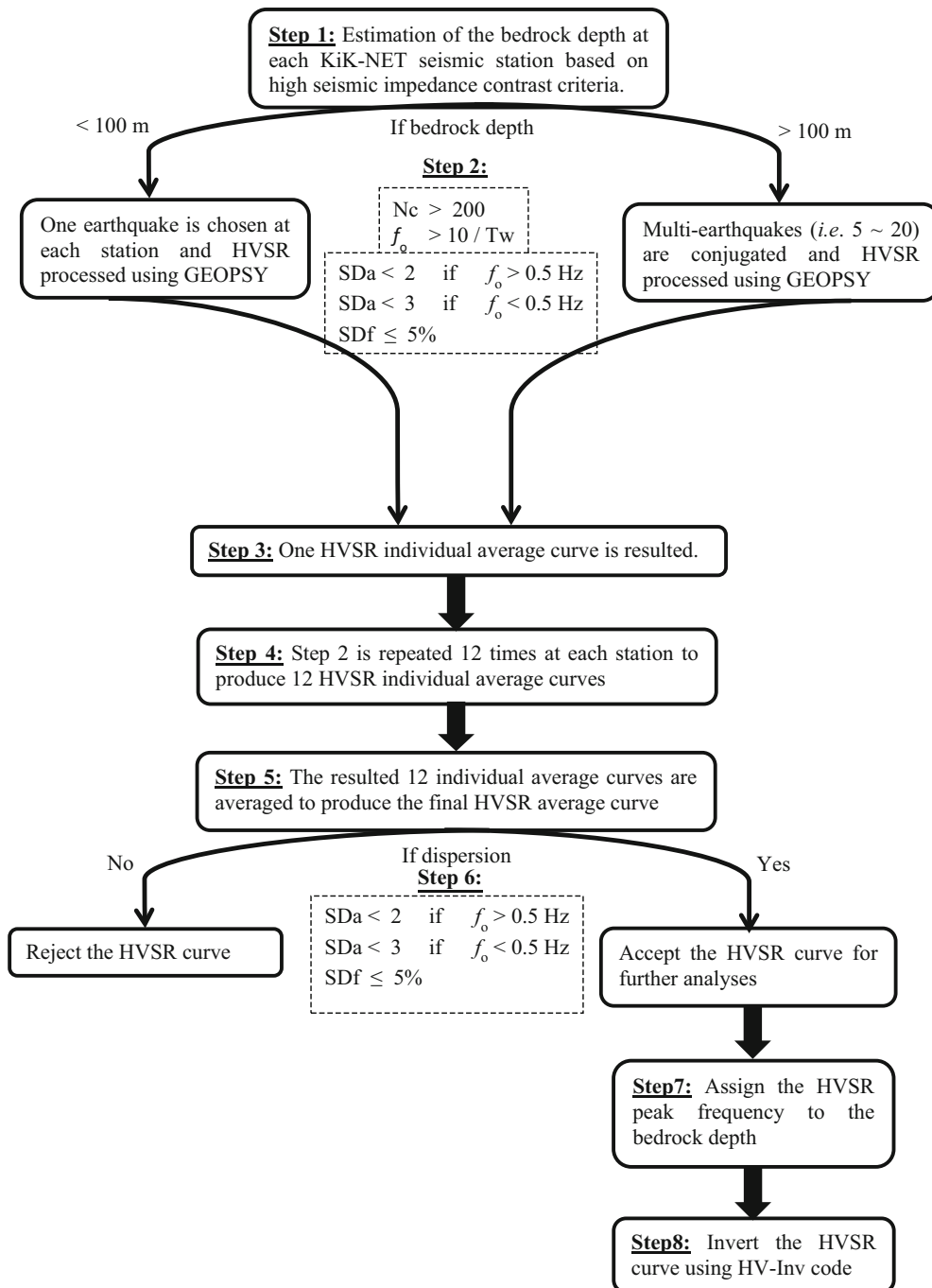


Figure 2
Diagram showing the systematic HVSR procedure

velocities for the soft, thin near-surface layers at the KiK-NET stations may be overestimated, because all KiK-NET stations have P -wave and S -wave velocity

structures derived from PS logging data. This velocity overestimation does not affect the reliability of the current bedrock interface determination, for three

main reasons. First, this overestimation is present only in *S*-wave velocities of the thin, soft, very near-surface layers. Second, *P*-wave velocities are not affected by this overestimation, so that IC_p is not biased. Third, this overestimation in thin near-surface *S*-wave velocity will decrease the calculated impedance contrast with respect to the underlying layer. As a result, the possibility of the presence of a bedrock interface will be excluded. However, the exclusion of the bedrock interface from further analyses is better than depending on a misinterpreted bedrock interface. Finally, the present *PS* logging seismic velocity structures of KiK-NET are considered reliable in this study. This reliability is evaluated and confirmed in the eighth and final step of this HVSR procedure.

2. Processing earthquakes using the Geopsy software suite (<http://www.geopsy.org>)

The reliability and quality of these HVSR calculations in this second step are assessed according to two basic requirements: (a) the expected fundamental resonance frequency of interest must be more than 10 significant cycles in each time window (T_w), and (b) the total number of significant cycles (N_c) must be greater than 200, and it is recommended that it be increased around two times at low fundamental resonance frequencies. In order to fulfill these two requirements, KiK-NET stations with bedrock depths less than 100 m are analyzed using the single earthquake approach, while for those with bedrock depths greater than 100 m, the multiple earthquakes approach is used, as shown in Figs. 3a and 4a, respectively. This is because the expected fundamental resonance frequencies of bedrock depths less than 100 m are higher than those of bedrock depths greater than 100 m, and vice versa.

3. Obtaining an individual average HVSR curve

Figures 3b and 4b show two examples for the resulting average HVSR curves. With the single earthquake approach, an average HVSR curve is calculated using the three-component records of one earthquake. At sites producing low fundamental resonance frequencies (i.e. ≤ 1 Hz), an HVSR-based technique is proposed to fulfill the second basic criterion of the total number of significant cycles. This

technique is known as the multiple earthquakes approach, and simply assumes several consequent earthquake records as a continuous time series to lengthen the total time window of each record, as previously shown in Fig. 4a. The conjunction points between each two adjacent earthquake records have a negligible effect on the resulting HVSR processing, because the frequencies of interest are low (i.e. ≤ 1 Hz). The resulting average HVSR curve from this step is considered the individual average HVSR curve. The third basic requirement for the reliability and quality of the present HVSR calculations is assessed in this step: acceptable low standard deviation values (i.e. low level of scattering), which may strongly affect the physical meaning of the HVSR peak frequencies. In this study, the standard deviations are calculated for the amplitudes of the time windows (SD_a) and for their peak frequencies (SD_f). According to Bard and the SESAME team (2004) guidelines, SD_a of less than 2 is recommended for peak frequencies (f_0) more than 0.5 Hz, or 3 for peak frequencies less than 0.5 Hz, within a frequency range between $0.5 f_0$ and $2 f_0$. The SD_f must be within a percentage of 5% to ensure that the peak frequencies of the individual averages appear at the same frequency on the HVSR individual average curves corresponding to the average \pm one standard deviation. This step is considered the first level in calculating the standard deviations.

4. Repeating the second and third steps 12 times to produce 12 individual average HVSR curves

This step is very important for obtaining the lowest dispersive results. Obviously, propagation path effects can strongly influence the resulting individual average HVSR curve. Propagation path effects are represented in shallow or deep earthquakes and far-field or near-field earthquakes. In other words, propagation path effects are proportionally dependent on the focal depth and epicentral distance of the earthquakes. In the present study, conditions of one-dimensional wave propagation oscillating in the vertical direction assuming plane-parallel are adopted throughout the analyses. Therefore, the recorded earthquakes at each KiK-NET site that fall into the deep and near-field category are selected to fulfill these conditions.

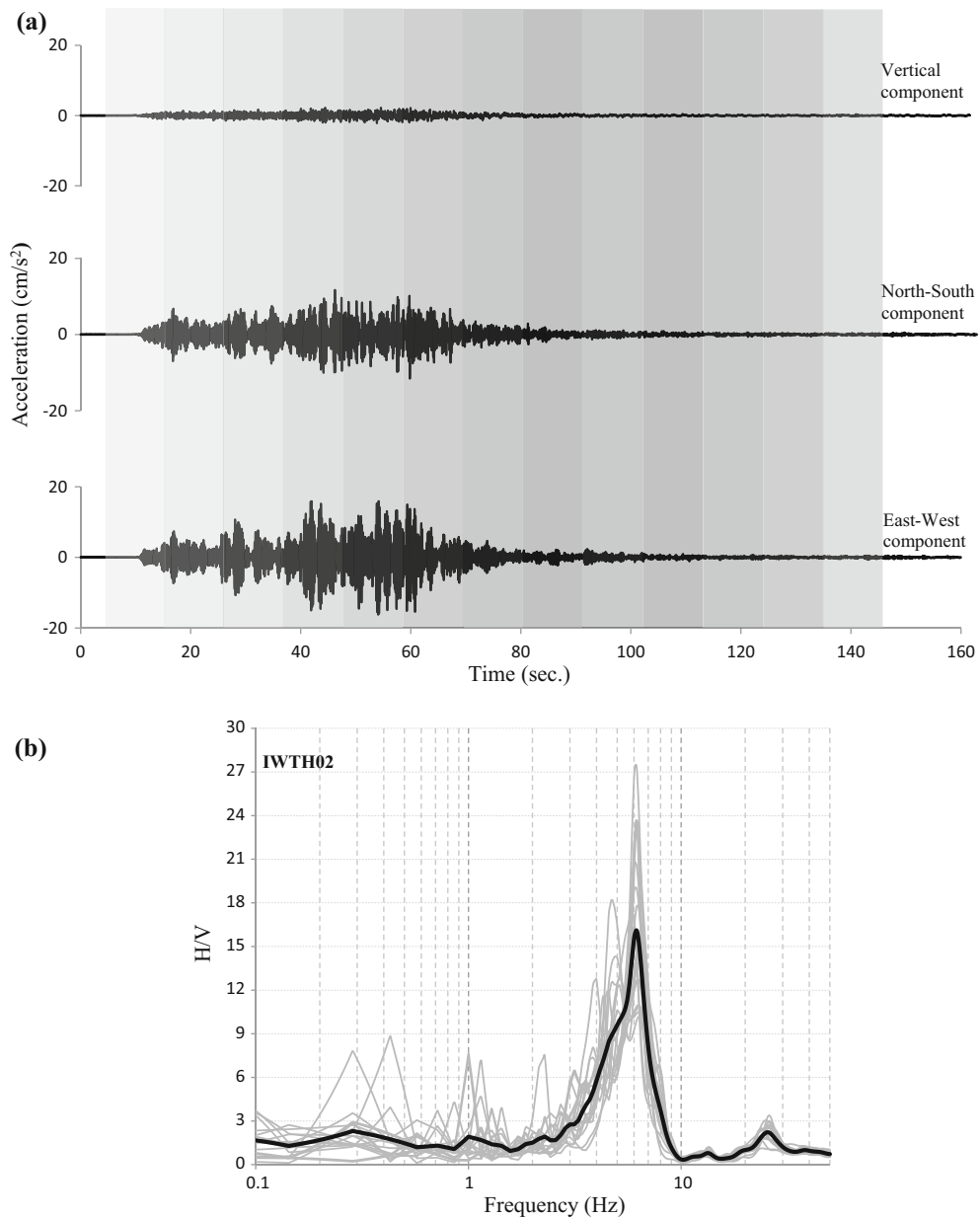


Figure 3

a Example of single earthquake records at the surface of the IWTH02 station showing time windows applied in Geopsy software. **b** The resulting individual average HVSR curves calculated by Geopsy are in thin gray lines, and the solid black line is the final average HVSR curve. (Note: calculated significant cycles \approx 910)

High standard deviation values mean that earthquakes used in the analyses are strongly non-stationary and undergo high scattering and perturbations, which may significantly affect the physical meaning of the HVSR peak frequencies. Therefore,

the HVSR measurements at each KiK-NET station are repeated 12 times using 12 earthquakes for cases of the single earthquake approach and 60–240 earthquakes for cases of the multiple earthquakes approach. This process ensures fulfillment of the third

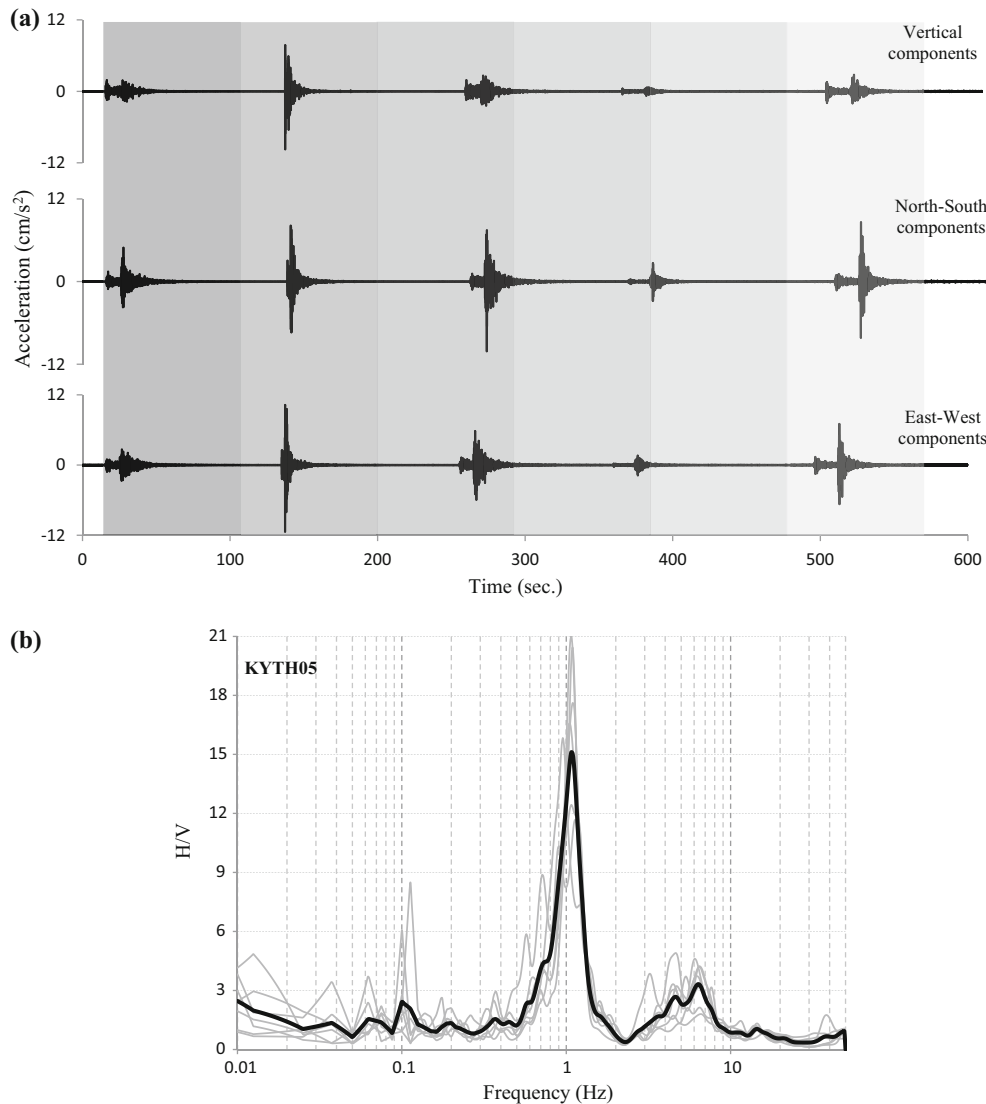


Figure 4

a Example of multiple earthquake records at the surface of the KYTH05 station showing the time windows applied in Geopsy software. **b** The resulting individual average HVSR curves calculated by Geopsy are in thin gray lines, and the solid black line is the final average HVSR curve. (Note: calculated significant cycles ≈ 590)

basic criterion of acceptable low standard deviation. As a result, 12 individual averages of HVSR curves are processed.

5. Calculating the final average HVSR curve by averaging the 12 individual average HVSR curves
6. Evaluating the dispersion level at each KiK-NET station

The standard deviations are calculated for the individual average HVSR curves following Bard and

the SESAME team (2004) guidelines that were explained in the third step. This step is considered the second level in calculating the standard deviations to ensure the lowest level of scattering. Calculating the standard deviations in both levels exceeds the recommendations of the framework of the European SESAME research project (Bard and SESAME team 2004) guidelines to avoid any dispersion in the resulting final HVSR curve. This means that the final average HVSR curve at each KiK-NET station must

undergo two subsequent levels of acceptable low standard deviation values. The first level considers the time windows applied on the single earthquake or multiple earthquakes approaches. The second level considers the resulting 12 individual averages of HVSR curves.

7. Assigning the HVSR peak frequency to the bedrock depth

This step is considered the most difficult and time-consuming step. However, the previously determined IC_p and IC_s are considered basic for assigning the HVSR peak frequency to its reliable bedrock interface or depth, as depicted in the two examples shown in Figs. 5 and 6. Figure 5a shows an example of deep bedrock depth. In this example, the second highest IC_p and the first highest IC_s directly indicate the bedrock interface. The first highest IC_p has very shallow depth, which is not consistent with the fundamental resonance frequency in Fig. 5b. In Fig. 6, the fundamental resonance frequency or the deep bedrock peak directly corresponds to the bedrock interface with the first highest IC_p and IC_s , whereas the secondary resonance frequency or the shallow bedrock peak corresponds to the bedrock interface with the second highest IC_p and IC_s . It is important to note that only clear and obvious fundamental and secondary resonance frequencies are assigned to their proper bedrock interfaces which are related to the first and second highest IC_p and IC_s . As a result, 360 out of the 684 KiK-NET stations are excluded from the present analyses due to difficulty and uncertainty in assigning accurate and proper bedrock interfaces or obtaining unclear HVSR peak frequencies.

8. Inverting the HVSR curves using HV-Inv code

The importance of this step is due to two reasons. The first is to check the reliability of *PS* logging seismic velocity structures of KiK-NET. The second is to check the reliability of the determined bedrock depth based on IC_p and IC_s . All the inversions performed were carried out using the HV-Inv code program (García-Jerez et al. 2016), which is specifically designed for forward calculation and inversion of the HVSR curves based on the diffuse field assumption (Sánchez-Sesma et al. 2011). Therefore,

30 KiK-NET seismic stations are selected to determine the inverted *P*-wave and *S*-wave velocity structures. Forward calculation for the HVSR curves were also carried out based on the original *PS* logging seismic velocity structures of KiK-NET. Finally, comparisons have been made between the observed, inverted, and forward calculated HVSR curves. The inverted velocity structures are compared with those obtained from KiK-NET.

5. Results and Discussion

5.1. HVSR Peak Frequencies

The identification of the fundamental HVSR peak frequencies met the Bard and SESAME team (2004) guidelines for clear and unique single HVSR peaks. Unclear frequency peaks such as cases of broad or multiple peaks are rejected because of the unfulfilled criterion of clear peaks. As a result, 324 KiK-NET stations in this study satisfy the clarity criterion according to Bard and the SESAME team (2004) guidelines. Cenozoic Quaternary and Cenozoic Neogene are the prevalent geologic ages at the 324 KiK-NET stations. Here it is interesting to note two significant observations. First, distribution of those 324 KiK-NET stations is not dependent on specific sites. Second, similarities in geologic ages indicate that geologic age factor is not a controlling factor that may affect the resulting fundamental resonance frequencies.

Figure 7 shows examples of some KiK-NET stations that are producing clear, sharp, and unique single HVSR peak frequencies of > 3 Hz, 3–1 Hz, and < 1 Hz, respectively. Basically, the characteristics of the clarity concept include the sharp amplitude of the HVSR peak and its relative value with respect to the HVSR value in other frequency bands, the standard deviation of the HVSR amplitude, and the standard deviation of HVSR peak frequency from individual averages.

At approximately 30 KiK-NET stations, the resulting HVSR curves exhibit two or multiple peaks. These are considered rare cases in this study. Examples are shown in Fig. 8. According to theoretical and numerical investigations, these cases occur

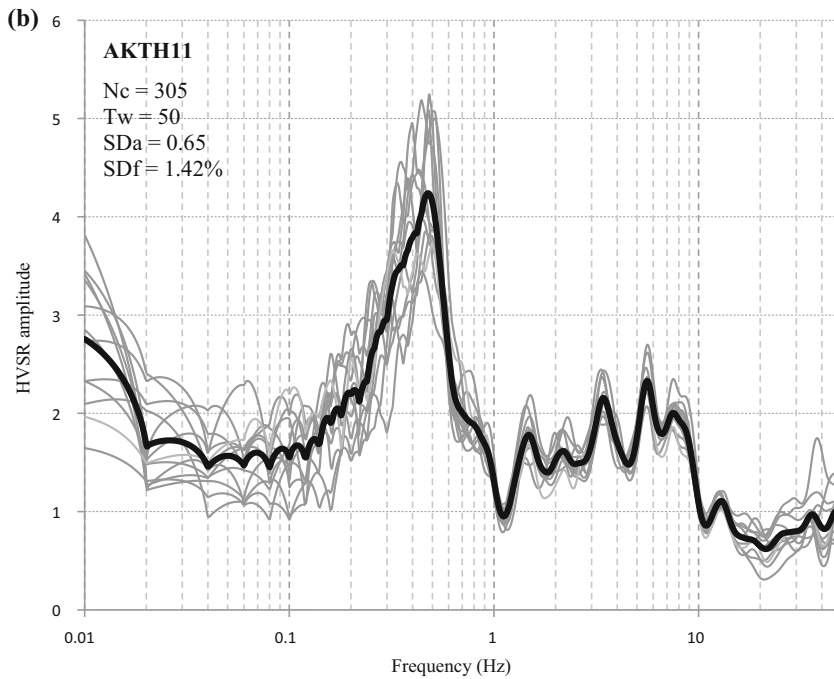
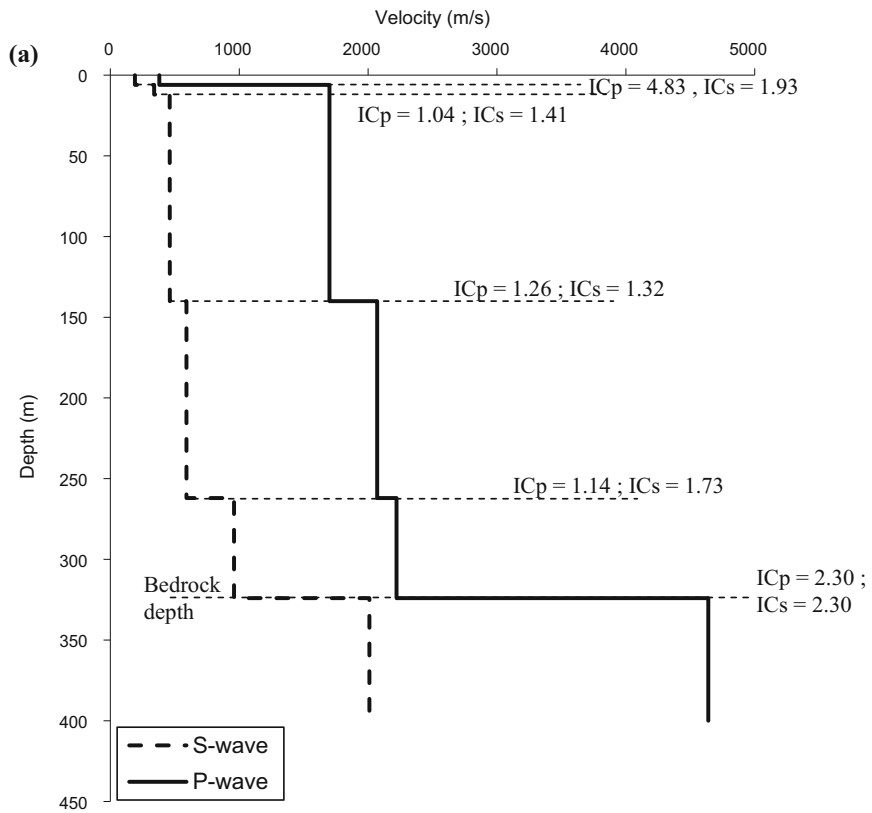


Figure 5
Example of bedrock depth assignment in the case of single HVSR fundamental peak

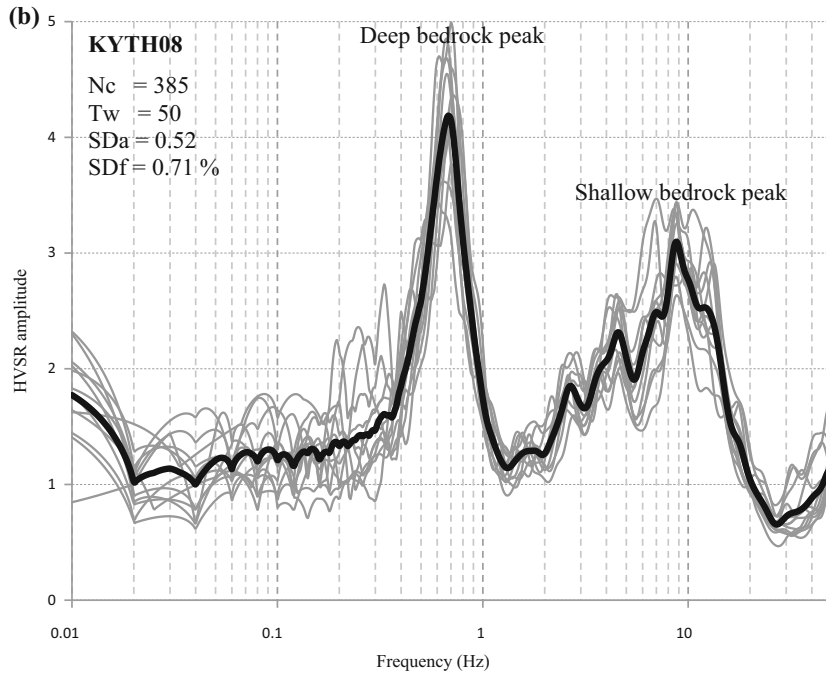
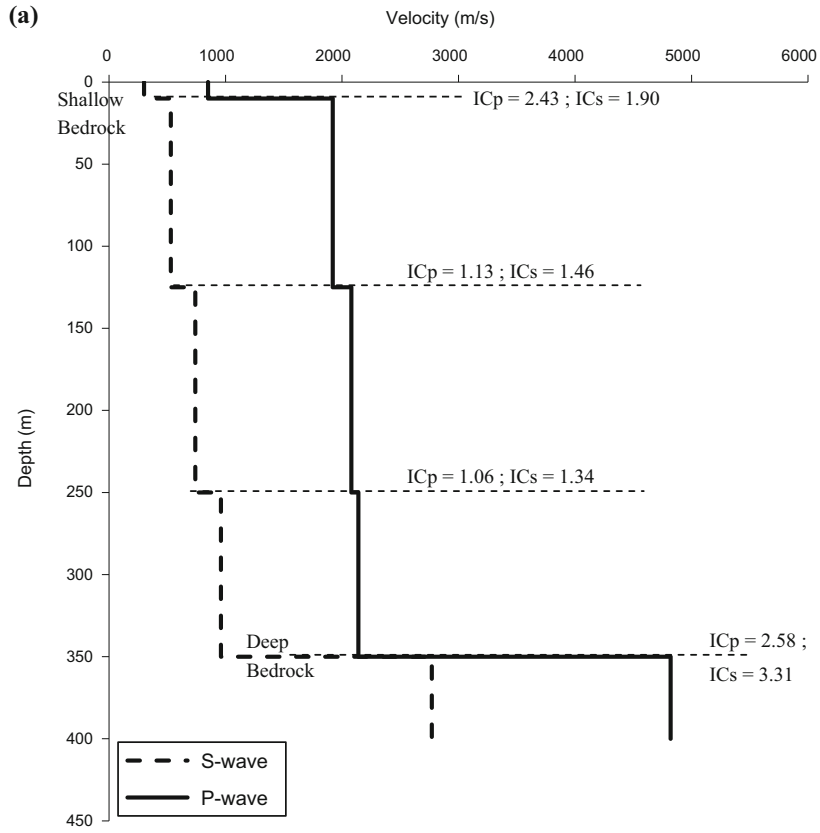


Figure 6
Example of bedrock depth assignment in the case of multiple HVSr fundamental peaks

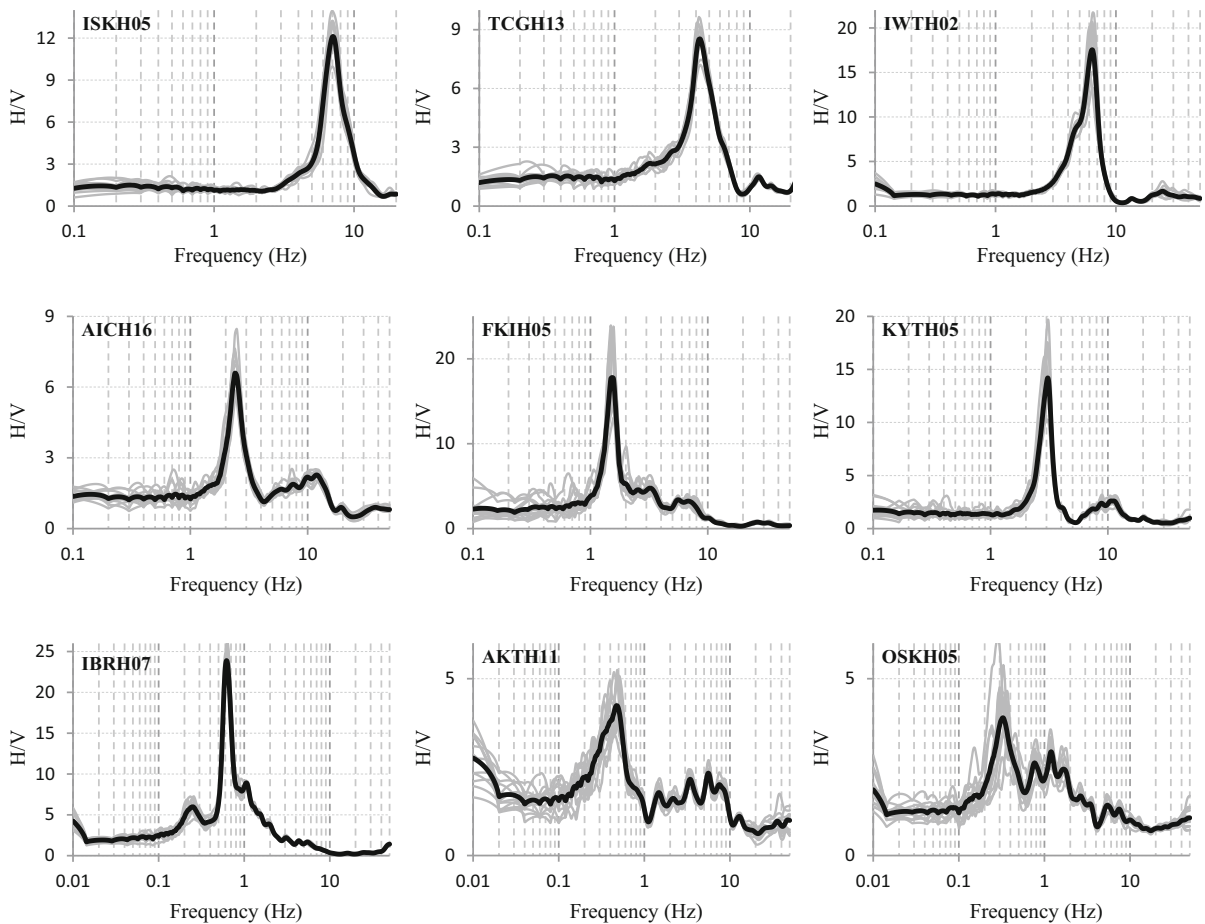


Figure 7

Examples of high, medium, and low HVSR peak frequencies (i.e. > 3 Hz, $3-1$ Hz, and < 1 Hz, respectively) at some KiK-NET stations (thin gray lines are the individual average HVSR curves, while the solid black line is the final average HVSR curve)

due to two or more large impedance contrasts. These impedance contrasts represent deep and shallow structures at different scales. In this study, some cases of two peaks are used in the present analyses due to ease of interpreting these peaks, whereas other cases are rejected due to significant difficulties in relating these peaks to their proper impedance contrast interfaces.

Figure 8 shows an examples of HVSR curves with unidentified peak frequencies, which are excluded from further analyses in the present study. There are many reasons for rejection in such cases. Some HVSR curves may exhibit a broad peak or a multiplicity of local maxima. Other HVSR curves show large standard deviations in the HVSR peak

frequencies of the individual averages. These cases strong affect the identification of clear HVSR peak frequencies. In this study, HVSR curves at 360 KiK-NET stations are excluded from the analyses because of their unclear HVSR peak frequencies.

The distribution of both the accepted and the rejected KiK-NET seismic stations is not influenced by different geological, sedimentological, topographical, or structural environments. The selected earthquakes in the present analyses fall into the deep- and near-field categories. Consequently, conditions of one-dimensional wave propagation oscillating in the vertical direction assuming plane-parallel are adopted throughout the analyses. Therefore, the lateral geological differences or inhomogeneities do not affect

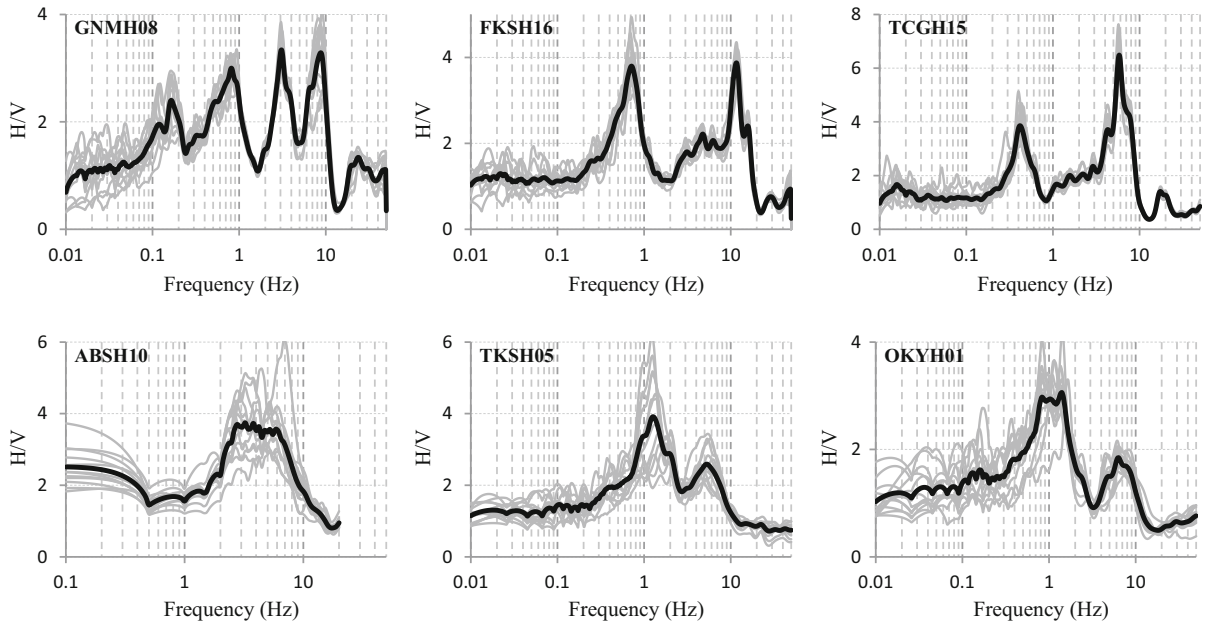


Figure 8

Examples of KiK-NET stations with two or multiple HVSR peak frequencies (upper), and rejected or unidentified HVSR peak frequencies (lower) (thin gray lines are the individual average HVSR curves, while the solid black line is the final average HVSR curve)

the resulting fundamental resonance frequencies. However, the accepted 324 KiK-NET seismic stations can be considered to represent simple geological conditions of one-dimensional velocity models, whereas the rejected 360 KiK-NET seismic stations represent more complex geological conditions.

HVSR peak frequency bands of > 3 Hz, 3–1 Hz, and < 1 Hz consist of 69, 17, and 14%, respectively, of the total accepted HVSR peak frequencies at the 324 KiK-NET stations. This indicates that most of the sites in Japan have large impedance contrasts that occur for shallow structures, whereas deep structures having strong impedance contrasts are very limited. However, the measured HVSR peak frequencies from the 324 KiK-NET stations can be considered sufficient enough data to establish robust frequency–bedrock depth relationships in Japan.

5.2. Frequency–Depth Relationship

Based on different lithological conditions, the 324 KiK-NET stations in this study are classified into two major categories: sedimentary and non-sedimentary.

For sites classified as sedimentary, the interface between the bedrock and the overlying layers lies within sedimentary layers or at the contact between sedimentary layers and basement rocks. For sites classified as non-sedimentary, the interface between the bedrock and the overlying layers lies within non-sedimentary layers such as igneous or metamorphic layers. The most interesting point is that the bedrock depths reach 2000 m and 700 m in sedimentary and non-sedimentary categories, respectively. Figure 9a shows a nonlinear regression fit in the sedimentary category to obtain the following equation:

$$h = 117.13f_{\text{HVSR}}^{-1.197} \quad (2)$$

Figure 9b shows three main parts in this nonlinear regression that is previously shown in Fig. 9a. The fundamental resonance frequency bands of > 3 Hz, 3–1 Hz, and < 1 Hz are dominant and characterize the bedrock depths of < 30 m, 30–100 m, and > 100 m, respectively. Scattering in the fundamental resonance frequencies at shallow bedrock depths (< 100 m) is very high, whereas a reasonable fit can be seen at bedrock depths > 100 m. The strong deviations of the data points at shallow bedrock

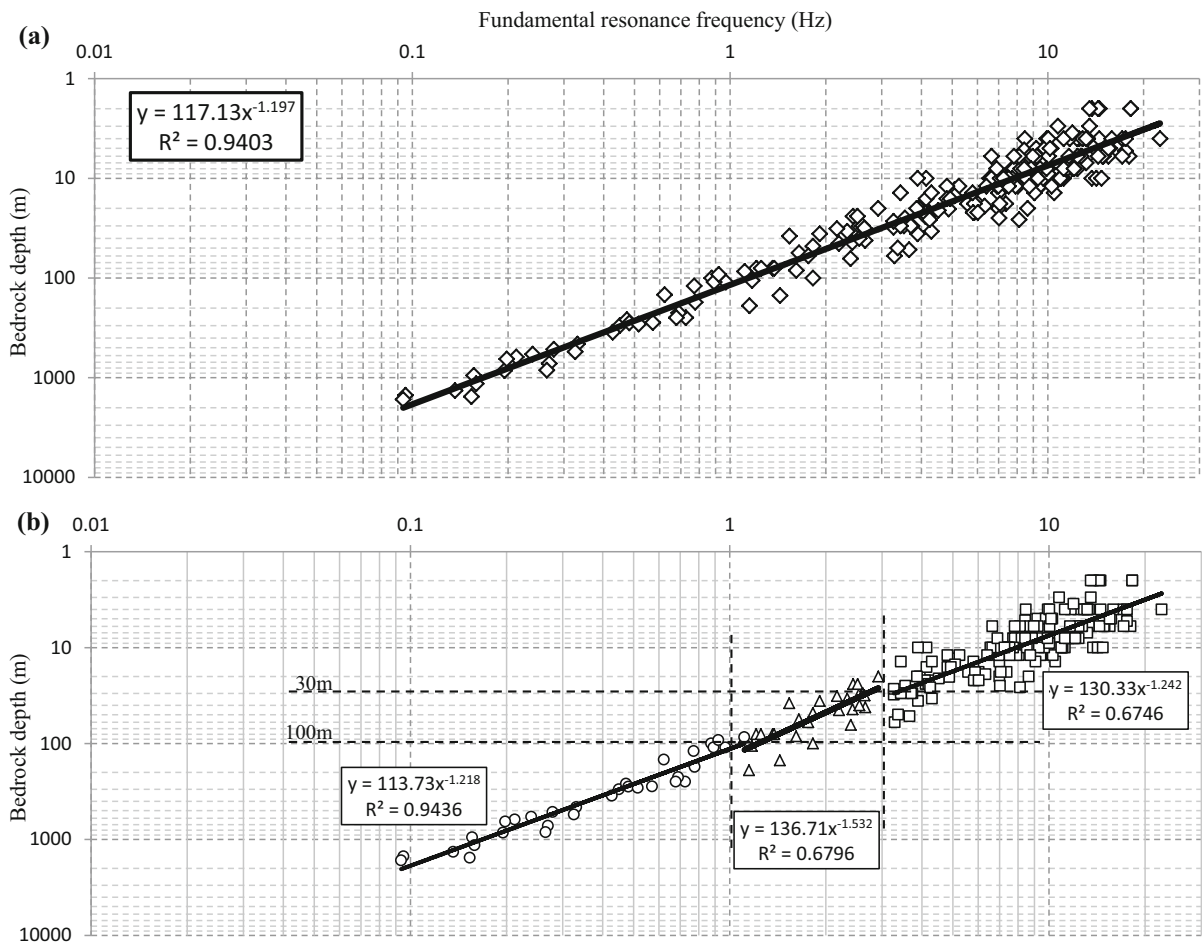


Figure 9

Fundamental resonance frequencies versus depth to bedrock in the sedimentary category. **a** Overall regression analyses. **b** Regression analyses for the main three parts

depths (< 100 m) from the general trend of the linear relationship are most likely a consequence of lithological inhomogeneities. This first observation indicates that the controlling part in the nonlinear regression relationship is the deeper part (> 100 m).

The dominant lithology in the non-sedimentary category consists mainly of tuff, pumice tuff, andesitic lava, granite, rhyolite, gabbro, granodiorite, basalt, gneiss, schist, and slate. Therefore, the non-sedimentary category is categorized to two subcategories depending on their origin. First, the igneous subcategory includes lithologies such as tuff, pumice tuff, andesitic lava, granite, rhyolite, gabbro, granodiorite, and basalt. Second, the metamorphic subcategory includes lithologies such as gneiss,

schist, and slate. Their resulting nonlinear regression analyses are shown in Fig. 10. Figure 10a shows high scattering in the fundamental resonance frequency versus bedrock depth, while Fig. 10b shows a reasonable fit. The nonlinear regression Eqs. 3 and 4 correspond to igneous and metamorphic subcategories, respectively.

$$h = 105.14f_{HVS}^{-0.899} \tag{3}$$

$$h = 132.67f_{HVS}^{-1.084} \tag{4}$$

The squared parameters (R_s) for Eqs. 2, 3, and 4 are 0.94, 0.62, and 0.90, respectively. Good correlation is found in the fundamental resonance frequency versus bedrock depth where the bedrock depth lies

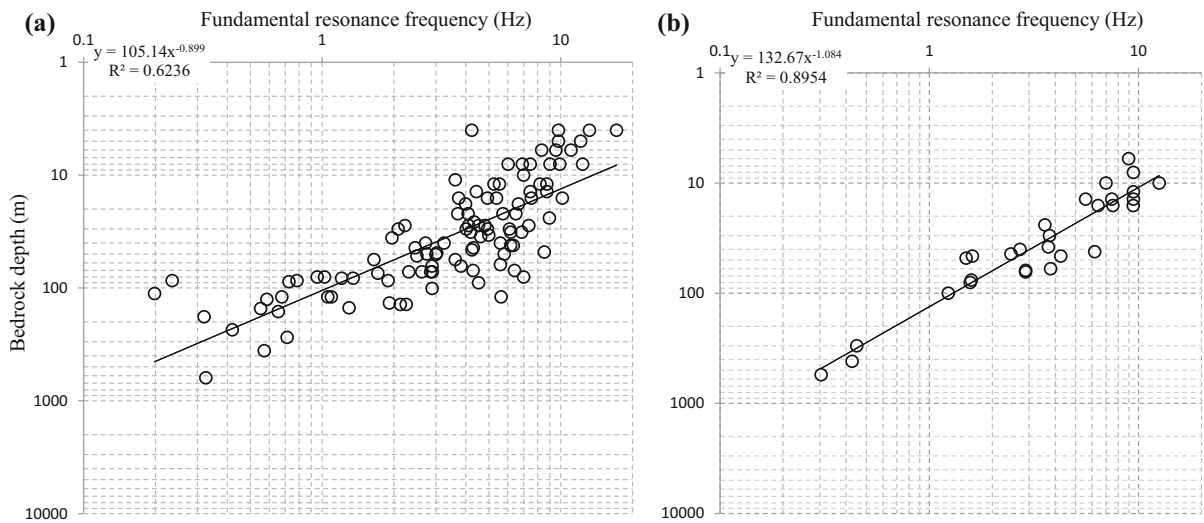


Figure 10

Fundamental resonant frequencies versus depth to bedrock in non-sedimentary subcategories. **a** Bedrock within igneous rocks. **b** Bedrock within metamorphic rocks

within sedimentary or metamorphic layers. High scattering prevails for the correlation where the bedrock depth lies within igneous layers. This observation indicates the strong effect of lithology on the frequency–depth relationships.

Generally speaking, it is known that engineering or geotechnical bedrock is characterized by shear wave velocity of between 300 m/s and 700 m/s, whereas seismic or seismological bedrock has shear wave velocity of between 3000 m/s and 3500 m/s. According to the site classification of NEHRP (FEMA 222A 1994; FEMA 450 2004) and IBC (2009), site class C is described as very dense soil and soft rock, where shear wave velocities are $360 \text{ m/s} < V_s \leq 760 \text{ m/s}$. Nath (2007) defined engineering bedrock as having shear wave velocity of 400 m/s to 700 m/s for the purpose of seismic microzonation. Miller et al. (1999) mapped bedrock by considering shear wave velocity of $\geq 244 \text{ m/s}$ as a value for bedrock using the MASW [Multichannel Analysis of Surface Waves] survey. Delgado et al. (2000b) considered shear wave velocity of $> 250 \text{ m/s}$ for the Triassic carbonate rocks and Triassic to Cretaceous limestones as geotechnical bedrock. In a study by Anbazhagan and Sitharam (2009), shear wave velocity of $330 \pm 30 \text{ m/s}$ was considered for the weathered rock and $760 \pm 60 \text{ m/s}$ for the

engineering bedrock. Sun (2014) considered shear wave velocities of $> 750 \text{ m/s}$ for most soft rock in Korea, which is the threshold value of engineering bedrock. Nath (2007) reported that seismic bedrock corresponded to shear wave velocity of $\geq 3000 \text{ m/s}$. Kawase et al. (2011, 2018) conducted detailed studies of one-dimensional shear wave velocity inversion using a diffuse field approach at 100 K-NET and KiK-NET stations using data for earthquakes and microtremors. They identified seismological or seismic bedrock, where shear wave velocity ranged between 3000 m/s and 3400 m/s. Satoh et al. (2001) carried out array microtremor and earthquake ground motion measurements in Sendai, Japan, to obtain the deep shear wave velocity structures inside the Sendai basin. They considered that seismic bedrock reached shear wave velocity of 3500 m/s.

In this study, the shear wave velocities determined for the bedrock varied according to differences in lithology. In the sedimentary category, the bedrock has shear wave velocities between 240 m/s and 3040 m/s. Igneous bedrock has shear wave velocities between 300 m/s and 3060 m/s, whereas metamorphic bedrock has shear wave velocities between 1000 m/s and 2900 m/s. In the present study, the bedrock at the majority of the KiK-NET stations is engineering bedrock, whereas at the other KiK-NET

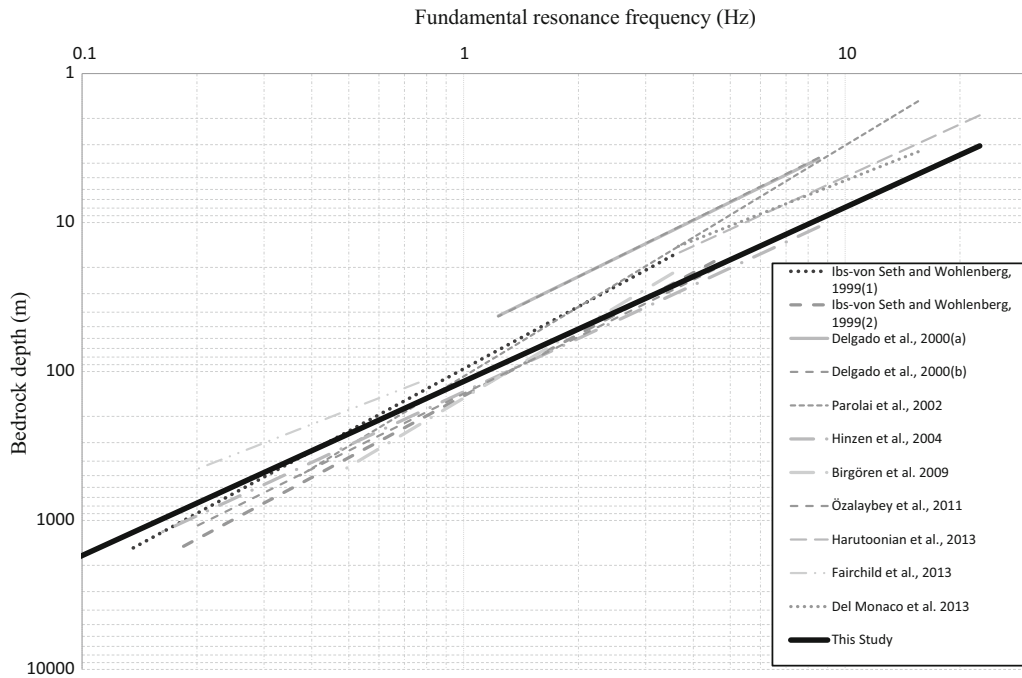


Figure 11 Comparison between the present study nonlinear regression relationship (Eq. 2) and previously established relationships

stations it is seismic bedrock. Therefore, it is practically useful to consider the bedrock depths determined in this study as bedrock.

For fundamental resonance frequencies greater than 10 Hz, the bedrock has a V_p/V_s range of 1.6–7.75. This wide range of V_p/V_s narrows as the fundamental resonance frequency reaches a value less than 0.1 Hz, where the bedrock has a V_p/V_s range of 1.6–2.2. Based on this criterion, the correlation of fundamental resonance frequency versus bedrock depth is rebuilt using only stations with a V_p/V_s ratio of the bedrock in the range of 1.6–2.2. Better fitting can be achieved with an R_S of 0.98. The new nonlinear regression fit can be obtained in Eq. 5.

$$h = 116.62f_{HVS}^{-1.169} \tag{5}$$

This criterion is also present in the non-sedimentary category. Rebuilding the correlations of the fundamental resonance frequency versus the bedrock depth for the igneous subcategory using only stations with a V_p/V_s ratio of bedrock in the range of 1.6–2.2 could not reproduce the correlations when compared with the overall correlations shown in Fig. 10a. In the

metamorphic subcategory, better fitting was achieved, with an R_S of 0.96, and a new nonlinear regression fit is obtained in Eq. 6.

$$h = 198.18f_{HVS}^{-0.894} \tag{6}$$

Previous regression relationships were established based on data taken from different sedimentary environments. Therefore, the nonlinear regression relationship of Eq. 2 is compared with previous relationships for the purpose of fair comparison, as shown in Fig. 11. It is clearly seen that the regression relationship in the present study has three differences in behavior when compared with previous relationships. First, the previous relationships underestimate the bedrock depths less than 30 m that correspond to fundamental resonance frequencies greater than 3 Hz. Second, these previous relationships overestimate the bedrock depths greater than 100 m that correspond to fundamental resonance frequencies less than 1 Hz. This underestimation at shallow depths and overestimation at greater depths could be related to the very local scale-based previous relationships. The third behavior is the marginally good agreement

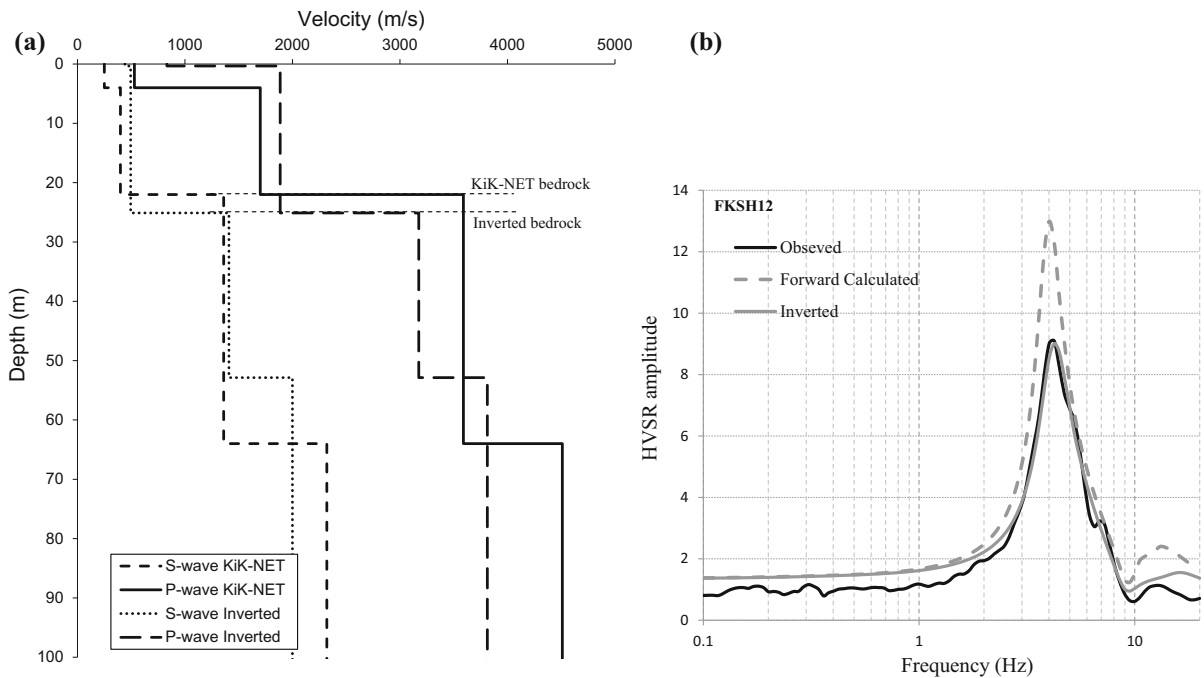


Figure 12

Example of HVSR inversion at the FKSH12 station. **a** KiK-NET and inverted velocity structures. **b** Observed, inverted, and forward calculated HVSR curves

between the present study regression relationship and the previous relationships around 1 Hz. This good agreement can be understood based on Eq. 1. The effect of the b parameter becomes negligible at 1 Hz, while the a parameter strongly controls the calculated depth. Therefore, the a parameter can be considered a site-specific parameter and would actually be a characteristic parameter for each region. As shown in Table 1, the b parameters have low variability, except for some cases (e.g. Fairchild et al. 2013; Del Monaco et al. 2013). The best-matched previous relationship with the present Eq. 2 is the relationship established by Hinzen et al. (2004). It is important to note that the maximum fundamental resonance frequency used in the study by Hinzen et al. (2004) is 2.5 Hz. This second observation also strongly indicates that the nonlinear regression relationship is governed and guided by the deeper part. This observation is very important, specifically in the case of using the frequency–depth relationship as a subsurface exploration tool. Based on this comparison, it can be concluded that geological conditions at

the site have a strong influence on the resulting frequency–depth relationship.

5.3. HVSR Inversion

In this section, 30 KiK-NET stations are selected in order to infer the velocity structures using HVSR inversion based on the diffuse field approach. The inverted velocity structures may provide an indication of the reliability of the KiK-NET velocity structures and the consequent inference of the bedrock depths. KiK-NET velocity structures provide the HVSR inversion process with an initial guess of the velocity structures and also range constraints for V_p and V_s to feed into the inverted velocity structures. Further, forward calculation of HVSR curves based on the original KiK-NET velocity structures are measured and superimposed on the observed and the inverted HVSR curves.

Figure 12 shows an example of HVSR inversion at the FKSH12 station. The inverted velocity structures are consistent with those provided from KiK-

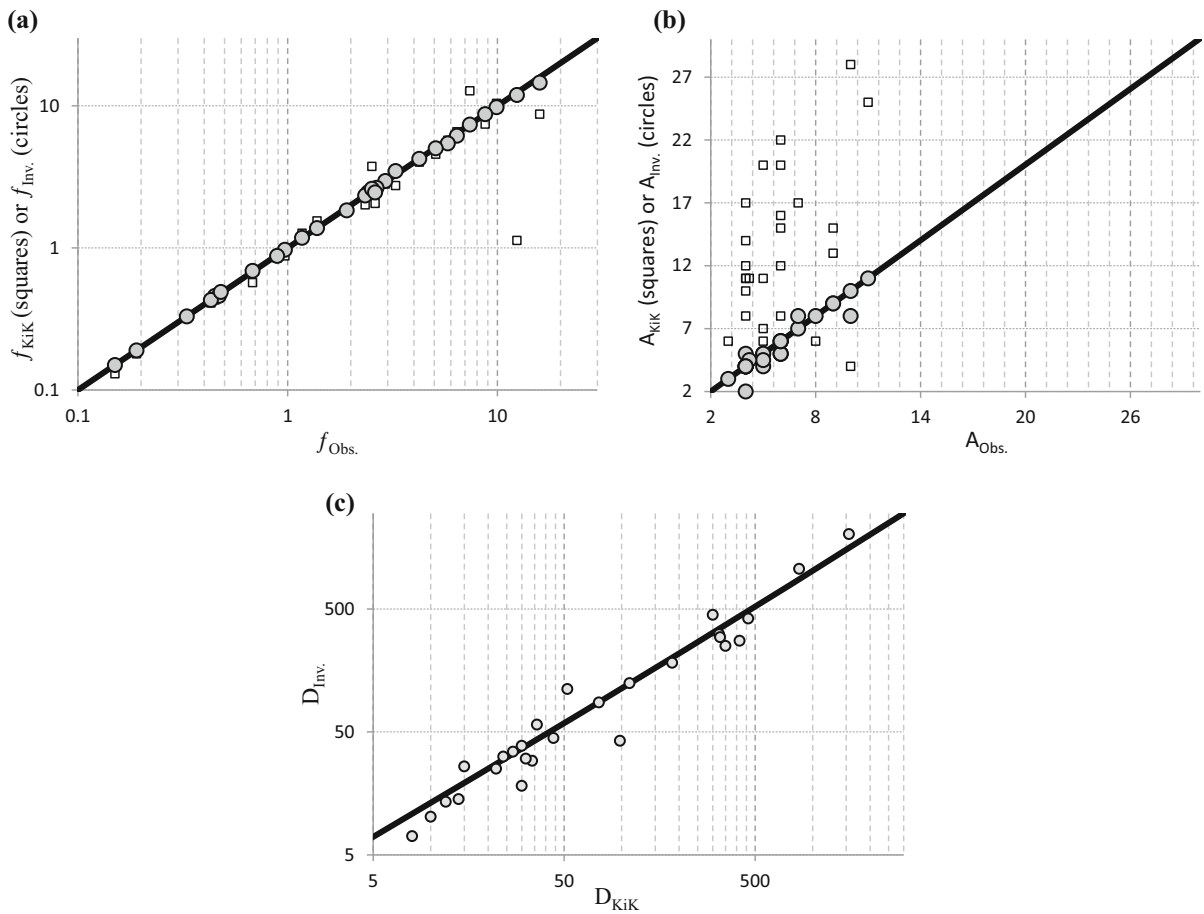


Figure 13

HVSr inversion performance. f_{Obs} , observed fundamental resonance frequency, f_{KiK} fundamental resonance frequency obtained from forward calculation using PS logging seismic velocity structures of KiK-NET, f_{Inv} , fundamental resonance frequency obtained from HVSr inversion, A_{Obs} , observed peak amplitude of HVSr, A_{KiK} peak amplitude of HVSr obtained from forward calculation using PS logging seismic velocity structures of KiK-NET, A_{Inv} , peak amplitude of HVSr obtained from HVSr inversion, D_{KiK} bedrock depth obtained from PS logging seismic velocity structures of KiK-NET, D_{Inv} , bedrock depth obtained from HVSr inversion

NET, as shown in Fig. 12a. Observed, inverted and forward calculated HVSr curves are thus superimposed in Fig. 12b.

Figure 13 presents an evaluation of the HVSr inversion with respect to peak amplitudes, fundamental resonance frequencies and bedrock depths. The observed fundamental resonance frequencies are fitted to those produced from the inverted and forward calculated HVSr curves as presented in Fig. 13a. Overestimation of the HVSr peak amplitudes, which are produced from forward calculation of HVSr curves based on KiK-NET velocity structures, is clearly observed when compared with those

produced from the HVSr inversion in Fig. 13b. Reasonable matching between bedrock depths identified from velocity structures of KiK-NET and HVSr inversion is presented in Fig. 13c. Table 2 summarizes the HVSr inversion results for the selected 30 KiK-NET stations, from high to low fundamental resonance frequencies (i.e. shallow to deep bedrock depths).

It is evident from the above analyses that the KiK-NET velocity structures, measured based on the PS logging suspension method, are reliable and may provide an indication that the present established frequency–depth relationships are also reliable. A

Table 2
HVSR inversion performance

	Station	Fundamental resonance frequency (Hz)			Peak HV amplitude			Bedrock depth	
		$f_{Obs.}$	f_{KiK}	$f_{Inv.}$	$A_{Obs.}$	A_{KiK}	$A_{Inv.}$	D_{KiK}	$D_{Inv.}$
Shallow bedrock < 30 m > 3 Hz	OITH08	15.90	8.74	14.57	4	47	2	4.0	0.7
	YMTH04	12.39	1.13	11.94	5	7	4	6.0	4.5
	SAGH02	9.90	10.41	9.78	6	8	5	8.0	7.1
	HYGH04	8.74	7.44	8.74	6	15	5	10.0	10.2
	OITH11	7.39	12.76	7.39	6	5	5	4.0	10.2
	SITH08	6.41	6.57	6.17	6	22	6	12.0	13.5
	SMNH03	5.80	5.73	5.45	8	6	8	14.0	14.2
	IBRH18	5.08	4.57	5.03	10	4	8	15.0	26.2
	FKSH12	4.24	4.02	4.24	9	13	9	22.0	25.1
	WKYH07	3.27	2.75	3.48	4	17	4	27.0	34.5
Medium bedrock 30 m → 100 m 3 Hz → 1 Hz	AICH16	2.42	2.52	2.46	7	17	7	44.0	44.6
	FKIH04	1.38	1.55	1.38	9	15	9	98.0	42.3
	FKSH14	1.17	1.27	1.18	5	11	5	52.0	111.7
	IBRH11	2.55	2.49	2.55	10	28	10	30.0	38.5
	KOCH12	2.92	2.82	2.96	3	6	3	76.0	86.8
	RMIH05	2.34	2.01	2.34	6	16	6	34.0	29.1
	KSRH10	1.91	1.89	1.84	6	20	6	36.0	57.3
	YMNH11	2.65	2.52	2.65	6	12	6	31.5	30.3
	YMGH14	2.52	3.75	2.61	7	31	8	24.0	31.5
	SOYH09	2.61	2.06	2.46	4	4	5	30.0	18.2
Deep bedrock > 100 m < 1 Hz	AICH04	0.45	0.43	0.46	5	20	5	300	448.6
	AICH14	0.97	0.88	0.97	4	11	4	184	182.6
	AKTH11	0.47	0.48	0.46	4	10	4	324	311.8
	CHBH13	0.19	0.18	0.19	4	14	4	850	1061
	FKOH07	0.43	0.41	0.43	5	6	4.5	415	276
	IBRH17	0.33	0.33	0.33	4	11	4	460	418.7
	KYTH08	0.68	0.57	0.69	4.2	11	4.5	350	250.6
	MYGH01	0.89	0.85	0.88	11	25	11	110	124.7
	OSKH02	0.15	0.13	0.15	4	12	4	1550	2034
	SZOH25	0.48	0.49	0.49	4	8	4	328	295.2

new, more recent interpretation of the HVSR curves is planned to be carried out on the present data to reduce the non-uniqueness of the inverted velocity structures. Diffuse field assumption links HVSR to Green's function retrieval through autocorrelation of the seismic field to estimate the layered velocity structure (e.g. Ducellier et al. 2013). The contribution from Lontsi et al. (2015) allows the use of a full microtremor HVSR spectrum for subsurface characterization using inversion based on diffuse wavefield theory. The authors optimized the inversion process by using a coarse integration step combined with the smoothing of the corresponding directional energy density (DED) spectrum, instead of using a smooth HVSR curve on a broad frequency range by considering a fine integration step, which is in turn time

consuming. Spica et al. (2018) also presented new theoretical and empirical results on computation and inversion of HVSR based on diffuse field assumption for combinations of receivers at surface and depth at the Groningen gas field. Therefore, adoption of these recent methods is planned to allow faster convergence towards reliable velocity structures at KiK-NET, and consequently reliable inference of the bedrock depths.

6. Conclusions

In this paper, a review of available nonlinear regression relationships between bedrock depth and fundamental resonance frequency is highlighted. New

nonlinear regression regional relationships based on a very dense network of seismic stations (KiK-NET) have been established. The horizontal-to-vertical spectral ratios (HVSR) of 10,000 weak earthquakes (i.e. linear events) were calculated at 684 KiK-NET stations in Japan, where geological, lithological, and *P*-wave and *S*-wave velocity structures are available from borehole drilling data for depths between 100 m and 3500 m. This paper makes several observations while analyzing the previous and the present nonlinear regression relationships. The stability of the HVSR of weak earthquakes is confirmed as a powerful geophysical tool for exploring bedrock depths in different lithological units of KiK-NET data. The frequency–depth relationship has a significant dependence on the lithological condition of the overlying layers/bedrock interface (i.e. sedimentary, igneous, or metamorphic). Frequency bands of > 3 Hz, 3–1 Hz, and < 1 Hz correspond to bedrock depths of < 30 m, 30–100 m, and > 100 m, respectively. The bedrock depths of < 30 m and 30–100 m show high scattering when correlated with the fundamental resonance frequencies, although they produce clear, unique, and single sharp HVSR frequency peaks. This strong scattering indicates that the impedance contrast of the overlying layers/bedrock interface is not the prominent factor controlling the frequency–depth relationship. Bedrock depths > 100 m show good and reasonable correlation. The general trend of the frequency–depth relationship is significantly controlled by the V_p/V_s ratio of the bedrock in the range of 1.6–2.2. The shear wave velocity of the bedrock has a negligible influence on the frequency–depth relationship. The present frequency–depth nonlinear regression relationships are strongly site-dependent. Therefore, it is suggested that these relationships be applied on other sites in Japan for further verification and assessment of reproducibility. Quantitative and reliable inferences between all the available relationships are needed in order to draw useful conclusions for finding reasonable data fitting of the geotechnical characteristics of the bedrock.

Acknowledgements

The author is very grateful to the National Research Institute for Earth Science and Disaster Prevention (NIED) for making the valuable KiK-NET data available. The author appreciates the valuable and constructive comments and suggestions from the editor and the reviewers.

Publisher's Note Springer Nature remains neutral with regard to jurisdictional claims in published maps and institutional affiliations.

REFERENCES

- Anbazhagan, P., & Sitharam, T. G. (2009). Spatial variability of the depth of weathered and engineering bedrock using multichannel analysis of surface wave method. *Pure and Applied Geophysics*, 166, 409–428. <https://doi.org/10.1007/s00024-009-0450-0>. (0033-4553/09/030409-20).
- Bard, P. Y., & SESAME team. (2004). Guidelines for the implementation of the H/V spectral ratio technique on ambient vibrations: Measurements, processing and interpretation, SESAME European research project, WP12—Deliverable D23. 12.
- Bindi, D., Parolai, S., Spallarossa, D., & Cattaneo, M. (2000). Site effects by H/V ratio: Comparison of two different procedures. *Journal of Earthquake Engineering*, 4, 97–113.
- Birgören, G., Özel, O., & Siyahi, B. (2009). Bedrock depth mapping of the coast south of İstanbul: Comparison of analytical and experimental analyses. *Turkish Journal of Earth Sciences*, 18, 315–329. <https://doi.org/10.3906/yer-0712-3>.
- Castro, R. R., Mucciarelli, M., Pacor, F., & Petrongaro, C. (1997). *S*-wave site response estimates using horizontal-to-vertical spectral ratios. *Bulletin of the Seismological Society of America*, 87, 256–260.
- Del Monaco, F., Tallini, M., De Rose, C., & Durante, F. (2013). HVNSR survey in historical downtown L'Aquila (central Italy): Site resonance properties vs. subsoil model. *Engineering Geology*, 158, 34–47. <https://doi.org/10.1016/j.enggeo.2013.03.008>.
- Delgado, J., Casado, C. L., Estévez, A., Giner, J., Cuenca, A., & Molina, S. (2000a). Mapping soft soils in the Segura river valley (SE Spain): A case study of microtremors as an exploration tool. *Journal of Applied Geophysics*, 45, 19–32.
- Delgado, J., Casado, C. L., Giner, J., Estévez, A., Cuenca, A., & Molina, S. (2000b). Microtremors as a geophysical exploration tool: Applications and limitations. *Pure and Applied Geophysics*, 157, 1445–1462.
- Ducellier, A., Kawase, H., & Matsushima, S. (2013). Validation of a new velocity structure inversion method based on horizontal-to-vertical (H/V) spectral ratios of earthquake motions in the Tohoku Area, Japan. *Bulletin of the Seismological Society of America*, 103(2A), 958–970.
- Fäh, D., Kind, F., & Giardini, D. (2001). A theoretical investigation of average H/V ratios. *Geophysical Journal International*, 145, 535–549.

- Fairchild, G.M., Lane, J.W., Voytek, E.B., & LeBlanc, D.R. (2013). Bedrock topography of western Cape Cod, Massachusetts, based on bedrock altitudes from geologic borings and analysis of ambient seismic noise by the horizontal-to-vertical spectral-ratio method, U.S. Geological Survey Scientific Investigations Map 3233, 1 sheet, maps variously scaled, p 17. Pamphlet, on one CD-ROM. <http://pubs.usgs.gov/sim/3233>. Accessed 20 Feb 2017.
- FEMA 222A. (1994). NEHRP recommended provisions for the development of seismic regulations for new buildings, 1994 edition, Part 1—provisions, Federal Emergency Management Agency
- FEMA 450. (2004). *NEHRP recommended provisions for seismic regulations for new buildings and other structures, 2003 edition, part 1—provisions* (p. 356). National Institute of Building Sciences, Washington, D.C.: Building Seismic Safety Council.
- Field, E. H. (1996). Spectral amplification in a sediment-filled valley exhibiting clear basin-edge-induced waves. *Bulletin of the Seismological Society of America*, 86, 991–1005.
- Field, E. H., & Jacob, K. (1993). The theoretical response of sedimentary layers to ambient seismic noise. *Geophysical Research Letters*, 20–24, 2925–2928.
- García-Jerez, A., Piña-Flores, J., Sánchez-Sesma, F. J., Luzón, F., & Perton, M. (2016). A computer code for forward computation and inversion of the H/V spectral ratio under the diffuse field assumption. *Computers & Geosciences*, 97, 67–78.
- Harutoonian, P., Leo, C. J., Tokeshi, K., Doanh, T., Castellaro, S., Zou, J. J., et al. (2013). Investigation of dynamically compacted ground by HVSR-based approach. *Soil Dynamics and Earthquake Engineering*, 46, 20–29. <https://doi.org/10.1016/j.soildyn.2012.12.004>.
- Hinzen, K. G., Weber, B., & Scherbaum, F. (2004). On the resolution of H/V measurements to determine sediment thickness, a case study across a normal fault in the lower Rhine Embayment, Germany. *Journal of Earthquake Engineering*, 8(6), 909–926. <https://doi.org/10.1080/13632460409350514>.
- IBC. (2009). The international building code, International Code Council, ISBN: 978-1-58001-725-1 (soft-cover edition), ISBN: 978-1-58001-724-4 (loose-leaf edition), pp 752.
- Ibs-von Seht, M., & Wohlenberg, J. (1999). Microtremors measurements used to map thickness of soft soil sediments. *Bulletin of the Seismological Society of America*, 89, 250–259.
- Kawase, H., Mori, Y., & Nagashima, F. (2018). Difference of horizontal-to-vertical spectral ratios of observed earthquakes and microtremors and its application to S-wave velocity inversion based on the diffuse field concept. *Earth, Planets and Space*, 70, 1. <https://doi.org/10.1186/s40623-017-0766-4>.
- Kawase, H., Sánchez-Sesma, F. J., & Matsushima, S. (2011). Application of the H/V spectral ratios for earthquake and microtremor ground motions. In: 4th IASPEI/IAEE international symposium: effects of surface geology on seismic motion, August 23–26, (2011), University of California Santa Barbara
- Lachet, C., & Bard, P. Y. (1994). Numerical and theoretical investigations on the possibilities and limitations of Nakamura's technique. *Journal of Physics of the Earth*, 42, 377–397.
- Lermo, J., & Chavez-García, F. J. (1993). Site effect evaluation using spectral ratios with only one station. *Bulletin of the Seismological Society of America*, 83, 1574–1594.
- Lermo, J., & Chavez-García, F. J. (1994). Are microtremors useful in site response evaluation? *Bulletin of the Seismological Society of America*, 84, 1350–1364.
- Lontsi, A. M., Sánchez-Sesma, F. J., Molina-Villegas, J. C., Ohrnberger, M., & Krüger, F. (2015). Full microtremor H/V(z, f) inversion for shallow subsurface Characterization. *Geophysical Journal International*, 202, 298–312. <https://doi.org/10.1093/gji/ggv132>.
- Maeda, T. (2004). Observatory shed effect on strong motion records identified by micro-tremor measurement, in *Proceedings of the thirteenth world conference on earthquake engineering*, Vancouver, British Columbia, Canada, Paper No. 568
- Miller, R. D., Xia, J., Park, C. B., & Ivanov, J. (1999). Multichannel analysis of surface waves to map bedrock. *The Leading Edge*, 18(12), 1392–1396.
- Mucciarelli, M. (1998). Reliability and applicability of Nakamura's technique using microtremors on the ground surface: an experimental approach. *Journal of Earthquake Engineering*, 2, 625–638.
- Nakamura, Y. (1989). A method for dynamic characteristics estimations of subsurface using microtremors on the ground surface. *Q Rep RTRI Jpn*, 30, 25–33.
- Nakamura, Y. (2000). Clear identification of fundamental idea of Nakamura's technique and its application, in *Proceedings of the XII world conference earthquake engineering*. Auckland, New Zealand, 8 pp
- Nath, S.K. (2007). Seismic microzonation framework—principles and applications, in *Proceedings of the workshop on microzonation*, Indian Institute of Science, Bangalore, 26–27 June 2007, India, pp. 9–35.
- Nogoshi, M., & Igarashi, T. (1970). On the propagation characteristics estimations of subsurface using microtremors on the ground surface. *Journal of the Seismological Society of Japan*, 23, 264–280.
- Nogoshi, M., & Igarashi, T. (1971). On the amplitude characteristics of microtremor (Part 2). *Journal of the Seismological Society of Japan*, 24, 26–40.
- Özalaybey, S., Zor, E., Ergintav, S., & Tapırdamaz, M. C. (2011). Investigation of 3-D basin structures in the İzmit Bay area (Turkey) by single-station microtremor and gravimetric methods. *Geophysical Journal International*, 186, 883–894. <https://doi.org/10.1111/j.1365-246X.2011.05085.x>.
- Parolai, S., Bormann, P., & Milkert, C. (2002). New relationships between V_s , thickness of sediments, and resonance frequency calculated by the H/V ratio of seismic noise for Cologne Area (Germany). *Bulletin of the Seismological Society of America*, 92, 2521–2527.
- Parolai, S., Richwalski, S. M., Milkereit, C., & Bormann, P. (2004). Assessment of the stability of H/V spectral ratios from ambient noise and comparison with earthquake data in the Cologne area (Germany). *Tectonophysics*, 390, 57–73.
- Sánchez-Sesma, F. J., Rodríguez, M., Iturrarán-Viveros, U., Luzón, F., Campillo, M., Margerin, L., et al. (2011). A theory for microtremor H/V spectral ratio: application for a layered medium. *Geophysical Journal International*, 186, 221–225.
- Satoh, T., Kawase, H., & Matsushima, S. (2001). Differences between site characteristics obtained from microtremors, S-waves, P-waves and codas. *Bulletin of the Seismological Society of America*, 91, 313–334.
- Spica, Z. J., Perton, M., Nakata, N., Liu, X., & Beroza, G. C. (2018). Site characterization at Groningen gas field area through joint surface-borehole H/V analysis. *Geophysical Journal International*, 00, 1–10. <https://doi.org/10.1093/gji/ggx426>.

- Sun, C. G. (2014). Earthquake engineering bedrock based on the shear wave velocities of Rock Strata in Korea. *The Journal of Engineering Geology*, 24(2), 273–281. <https://doi.org/10.9720/kseg.2014.2.273>.
- Tün, M., Pekkan, E., Özel, O., & Guney, Y. (2016). An investigation into the bedrock depth in the Eskisehir Quaternary Basin (Turkey) using the microtremor method. *Geophysical Journal International*, 207(1), 589–607. <https://doi.org/10.1093/gji/ggw294>.
- Yamanaka, H., Takemura, M., Ishida, H., & Niwa, M. (1994). Characteristics of long-period microtremors and their applicability in exploration of deep sedimentary layers. *Bulletin of the Seismological Society of America*, 84, 1831–1841.
- Yoshimura, C., Hibino, H., Uchiyama, Y., Maeda, T., Kurauchi, N., & Aoi, S. (2003). Vibration characteristics of the observation house at KiK-net Hino, Japan Earth and Planetary Science Joint Meeting (**in Japanese with English abstract**).

(Received October 17, 2018, revised June 7, 2019, accepted June 13, 2019, Published online June 26, 2019)